Solid State Ionics 335 (2019) 15–22

Contents lists available at ScienceDirect

Solid State Ionics

journal homepage: www.elsevier.com/locate/ssi

An alluaudite compounds $Na_2Fe_2(SO_4)_3$ vs. $Na_{2.5}Fe_{1.75}(SO_4)_3$ as earth abundant cathode materials for Na-ion batteries

Anna Plewa*, Andrzej Kulka, Dominika Baster, Janina Molenda

AGH University of Science and Technology, Faculty of Energy and Fuels, al. Mickiewicza 30, 30-059 Krakow, Poland

ARTICLE INFO

Keywords:
Na-ion batteries
Cathode material
$Na_{2+2y}Fe_{2-y}(SO_4)_3$
Electrochemical properties

ABSTRACT

In this paper, two compounds $Na_2Fe_2(SO_4)_3$ and $Na_{2.5}Fe_{1.75}(SO_4)_3$ cathode materials were synthesised and studied in terms of their structural, transport and electrochemical properties in $Na/Na^+/Na_{2+2y}Fe_{2-y}(SO_4)_3$ (y = 0; 0.25) cells. The materials were fabricated using a low temperature solid state reaction. XRD measurements accompanied with Rietveld analysis confirmed the presence of a phase with C2/c symmetry for both obtained compositions. By changing the stoichiometry and synthesis conditions of $Na_{2+2y}Fe_{2-y}(SO_4)_3$ the compound with a minimal amount of impurities can be obtained. $Na_{2.5}Fe_{1.75}(SO_4)_3$ material exhibits good transport properties with low charge transport activation energy. Electrochemical studies show improved performance of $Na_{2.5}Fe_{1.75}(SO_4)_3$ compared to $Na_2Fe_2(SO_4)_3$.

1. Introduction

The types of batteries application can be divided into two categories. First where the volumetric energy density of the batteries plays the critical role such as in portable electronic devices, electrical and hybrid electric vehicles. And the second group where volumetric energy density is less demanding as in systems storing electric energy incorporated within wind or solar power grids. Large-scale energy storage systems have emerged as an important challenge facing the 21st century and it is now evident that in order to achieve green and sustainable energy development, large battery units storing energy from renewable resources power plants should be developed [1–3]. One of the most promising candidate for the realization of such solutions is the Na-ion batteries technology, due to the many advantages of sodium. It ranks as the world's 4th most widely abundant element on earth and is also a worthy candidate in the secondary battery field because of its encouraging electrochemical properties [4]. For these reasons using Na-ion batteries allows creating new, economical and ecofriendly large-scale power storage systems. This inspires the search for the novel electrode materials for innovative sodium batteries, especially basing on earth-abundant and ecofriendly elements. Particularly, in order to enhance gravimetric and volumetric energy density of Na-ion batteries, the cathode materials with an appropriate crystal structure, 3d metal redox potential, high electrical conductivity, and sodium intercalation kinetics should be evaluated. The very promising group of cathode materials are polyanion compounds combing tetrahedral units $(XO_4)^{n-}$ with MO_6 polyhedra [5]. Because of the strong covalent bonding in $(XO_4)^{n-}$, polyanion materials exhibit high structural stability, which makes them especially interesting for commercial applications [6]. One of the most prospective candidates from this group basing on economical and abundant elements Na-Fe-S-O, is $Na_2Fe_2(SO_4)_3$ firstly reported in 2014 [7]. $Na_2Fe_2(SO_4)_3$ forms a unique structure with alluaudite type framework [8]. In a standard representation the alluaudite type compounds can be written as $AA'BM_2(XO_4)_3$, where three different crystallographic positions: A, A' and B are occupied by sodium ions (Na1-B, Na2-A, Na3-A') while M site is occupied by Fe and X by S [9]. Within this structure, FeO_6 octahedrons are edge connected and form a Fe_2O_{10} units and share corners with SO_4^{2-} tetrahedrons. SO_4^{2-} units also residue in two different crystallographic positions (S1 and S2) which has different alignment in relation to Fe_2O_{10} pairs. Such arrangement results in a three-dimensional network, characterised by the existence of the open channels along the *c* crystallographic direction in which Na ions may diffuse [8–10].

$Na_2Fe_2(SO_4)_3$ exhibits the highest so far found Fe^{3+}/Fe^{2+} redox potential equal 3.8 V vs. Na/Na^+, its theoretical energy density is particularly large (456 Wh kg^{-1} vs. Na/Na^+). It seems to be enough to make Na-ion batteries competitive with Li-ion analgue. Another favourable feature of $Na_2Fe_2(SO_4)_3$ is its monotonous discharged curve outstretching between 4 and 3 V vs. Na^+/Na^0.

Despite the superior electrochemical performance of this alluaudite type material, it is difficult to obtain the stable phase of $Na_2Fe_2(SO_4)_3$ [7], partially because of its decomposition at moderate temperatures,

* Corresponding author.
E-mail addresses: annap@agh.edu.pl (A. Plewa), molenda@agh.edu.pl (J. Molenda).

https://doi.org/10.1016/j.ssi.2019.02.007
Received 18 June 2018; Received in revised form 29 January 2019; Accepted 7 February 2019
Available online 21 February 2019
0167-2738/

instability in the water conditions as well as the tendency of iron ions to oxidise in an air atmosphere.

Recent reports have indicated that low temperature solid state synthesis method gives the opportunity to obtain the $Na_2Fe_2(SO_4)_3$ powder with the relatively low amount of impurities (17 wt% of Fe_2O_3 and $FeSO_4$). In the mentioned method, a mixture of dried $FeSO_4$ grounded with Na_2SO_4 was prepared in an argon atmosphere. Then substrates were annealed at 350 °C for 1 day under Ar atmosphere. It was also demonstrated that synthesis of off-stoichiometric alluaudites $Na_{2+2y}Fe_{2-y}(SO_4)_3$, where y is approximately 0.25–0.3, leads to decreasing of the amount of the secondary phases (in form of Fe_2O_3) to 3 wt% [10].

Moreover, the $Na_{2+2y}Fe_{2-y}(SO_4)_3$ compounds even with low amount of impurities are not able to reach their theoretical capacity probably due to their low electrical conductivity and existence of the secondary phases. Therefore, it is desirable to determine the optimal synthesis conditions leading to the production of the pure phase $Na_{2+2y}Fe_{2-y}(SO_4)_3$ compounds and define electrochemical parameters limiting their performance.

This paper presents fundamental studies regarding the influence of the stability of precursor $FeSO_4$ - Na_2SO_4 and atmosphere conditions upon heat treatment on the phase composition of synthesised $Na_{2+2y}Fe_{2-y}(SO_4)_3$ samples. Results can be used to further optimise the synthesis conditions for other materials based on Fe-Na-S-O elements including kröhnkite- and alluaudite-type structures. Obtaining of $Na_{2+2y}Fe_{2-y}(SO_4)_3$ compositions were confirmed by detailed investigation of the structural properties using XRD method. For the first time in the published papers, the grains size distribution of $Na_{2.5}Fe_{1.75}(SO_4)_3$ is presented. SEM studies indicate that the obtained material is nanometric size powder with smaller grains than previously reported. Moreover, electrical conductivity research and the analysis of the sodium ion diffusion coefficient are presented, complementing the previously reported computer modeling of Na^+ transport during intercalation/deintercalation processes. We also present the analysis of electrochemical properties for the selection of the optimal electrolyte for $Na/Na^+/Na_{2+2y}Fe_{2-y}(SO_4)_3$ cells.

2. Experimental

2.1. Synthesis conditions

The $Na_{2+2y}Fe_{2-y}(SO_4)_3$ (y = 0; 0.25) were synthesised through a low temperature solid state reaction method. Firstly, the dehydrated $FeSO_4$ was obtained by calcination of $FeSO_4{\cdot}7H_2O$ (Kanto Chemical Co., 99%) in 5 vol% H_2 in Ar at 300 °C for 12 h. $FeSO_4$ and anhydrous Na_2SO_4 (Wako, 99%) were ball-milled three times for 30 min in a SPEX SamplePrep 8000D mixer/mill in zirconia vials with isopropanol, and dried at 100 °C. The final heat treatment of the precursors was carried out at 350 °C for 24 h in an inert or reducing atmosphere. In order to obtain stoichiometric phase $Na_2Fe_2(SO_4)_3$ three different atmospheres (Ar, Ar + 1%H_2 and Ar + 5%H_2) were used. Whereas for $Na_{2.5}Fe_{1.75}(SO_4)_3$ strongly reductive gas mixture (Ar + 5%H_2) was used.

2.2. Thermal stability

Thermal stability of milled precursor ($FeSO_4$ and Na_2SO_4) was measured on TA Q5000 IR thermobalance. For the experiments, 30–50 mg of the studied powder was placed on a Pt holder and heated at 25 °C–500 °C temperature range (5° min^{-1} heat rate) with a gas flow 5 vol% H_2 in Ar of 100 cm^3 min^{-1}. The mass spectrometer was used to determine the side gases of the reactions during the heating process. The test was conducted on a custom-made setup comprising a furnace, a gas supply system with mixer and mass flow controllers, U-tube quartz sample holder with an inner diameter of the catalytic bed zone of 15 mm, and Pfeiffer Vacuum ThermoStar mass spectrometer.

2.3. Structural and morphology studies

The crystal structure of the obtained materials was investigated by means of X-ray diffraction (XRD) technique carried out with PANalytical Empyrean diffractometer equipped with a CuK_α radiation source and a Pixcell3D detector. Diffraction patterns were obtained in the 10–110° 2θ range. Phase analysis was based on the matching pattern with PDF4+ (2015) database records. The parameters of the crystal structure were refined using the Rietveld method with the GSAS/EXPGUI software package [11–13]. The morphology of the selected powder was investigated by means of Scanning Electron Microscope (SEM) technique with the SEM FEI Nova Nano SEM200. The grain size distribution was measured with Mastersizer 3000 laser diffraction particle size analyser. Inductively coupled plasma atomic emission spectroscopy ICP (spectrometer PerkinElmer Optima 5300V) was used for check the amount of Na and Fe in the synthesised material.

2.4. Electrical and electrochemical studies

Electrical conductivity was measured at the temperature range 25 °C–400 °C, with 10 °C steps during cooling and heating, by means of impedance spectroscopy method using Solartron 1260 frequency response analyser with sinusoidal excitation voltage equal 0.2 V. For the measurement the pellet of synthesised $Na_{2.5}Fe_{1.75}(SO_4)_3$ (d = 12 mm; h = 2 mm) was used. Their relative density was estimated as 77%. To ensure good electrical contact between the sample and the electrodes, Au was sputtered on each side of a polished disk sample. The resistance values were calculated by fitting the substitution circuit to the impedance spectra which consisted of a parallel capacitor and a resistor.

Electrochemical studies were carried out in $Na/Na^+/Na_{2+2y}Fe_{2-y}(SO_4)_3$ (y = 0; 0.25) cells. Three types of electrolytes were used: the 1 M solution of $NaPF_6$ (Sigma-Aldrich, 99,99%) in 1:1 mixture of ethylene carbonate (EC, Sigma-Aldrich, 99,99%) and diethyl carbonate (DEC, Sigma-Aldrich, 99,99%), the 1 M solution of $NaPF_6$ (Sigma-Aldrich, 99,99%) in propylene carbonate (PC, Sigma-Aldrich, 99,7%), the 1 M solution of $NaClO_4$ (Sigma-Aldrich, 99,99%) in propylene carbonate (PC, Sigma-Aldrich, 99,7%). Sodium metal was used as a negative electrode. For the positive electrode, the active material $Na_{2+2y}Fe_{2-y}(SO_4)_3$ (80 wt%), was mixed with polyvinylidene difluoride (PVDF) binder (10 wt%), with an addition of carbon black (10 wt%). For the preparation of the slurry, *N*-methyl-2-pyrrolidone (NMP) was added, in order to obtain the proper viscosity. The prepared slurries were coated on Al foil and dried at 70 °C in a vacuum dryer. The positive electrodes, cut in a form of 12 mm-diameter discs, were dried again at 80 °C for 12 h in vacuum. Coin-type CR2032 electrochemical cells were assembled in a glove box (UNILAB, M. Braun) under argon atmosphere, with controlled oxygen and water vapor pressure (< 0.1 ppm). Charge/discharge curves were recorded on ATLAS PGStat 0361 galvanostat/potentiostat in 2.0–4.5 V range, with C/10 current rates. Cyclic voltammetry studies were carried out using Autolab PGSTAT302 with scanning rate equal 0.01 mV s^{-1}, 0.1 mV s^{-1} and 0.5 mV s^{-1} in 2–4.5 V voltage range.

3. Thermal analysis of Na_2SO_4 - $FeSO_4$ precursor

In order to precisely determine the range of temperatures in which the reactions during the synthesis of $Na_2Fe_2(SO_4)_3$ occur the thermogravimetric analysis of the mixture of the precursors was carried out. Fig. 1 shows the mass evolution of Na_2SO_4 - $FeSO_4$ mixture in a harsh atmosphere of 5%H_2 in Ar as a function of temperature. At the beginning of the experiment, between 50 °C and 270 °C, mass loss was observed on the TG curve. Taking into consideration the simultaneous increase of the ionic current corresponding to the H_2O molecules (m/z = 18) the mass drop can be attributed to desorption of water from surface area of the substrates and at higher temperatures the release of the traces of crystal water present in $FeSO_4{\cdot}7H_2O$. Although all

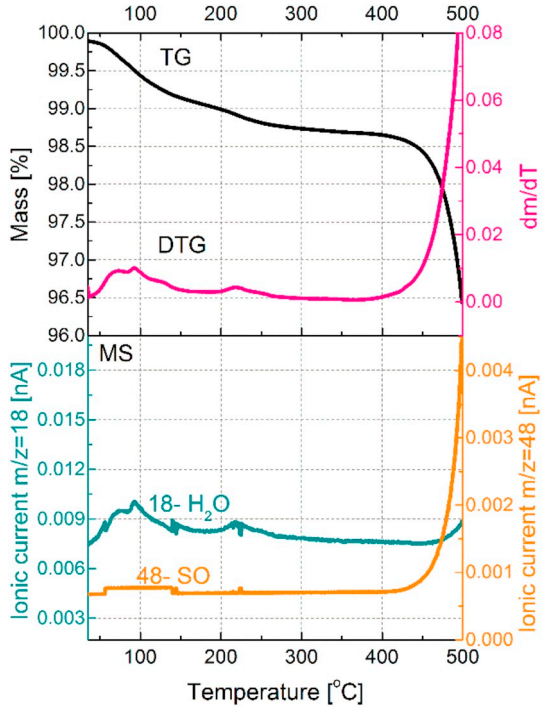

Fig. 1. Thermogravimetric measurement of Na_2SO_4 - $FeSO_4$ mixture correlated with mass spectrometry.

substrates used for synthesis should not contain any H_2O, because $FeSO_4{\cdot}7H_2O$ was heating according to literature data to complete dehydration and anhydrous Na_2SO_4 was stored in a protective atmosphere, it is evidence that water traces are still present during the heating of the precursors. It can be assumed that this quantity of water can result from hydration of Na_2SO_4 - $FeSO_4$ mixture during ball-milling or incomplete dehydration of $FeSO_4$.

Between 300 °C and 400 °C the preservation of the mass of the substrates is observed without production of any gaseous side products. However, when the temperature exceeds 400 °C the rapid mass decline is detected, at the same time mass spectrometry measurements revealed proportionally increase of the ionic current (m/z = 48, 40, 32 and 64) indicating the formation of the gaseous sulfur dioxide SO_2. The thermal stability of alkaline earth sulfates has been already studied in the literature and it was found that $FeSO_4$ in the air starts to decompose to hematite (α-Fe_2O_3) above 500 °C [14,15] while in case of the Na_2SO_4, the decomposition in the air atmosphere starts at 850 °C [16,17]. In the present study, the mixture of Na_2SO_4 - $FeSO_4$ substrates starts to decompose at 400 °C which is relatively lower compared with a temperature of the decomposition of the sole substrates. It may indicate that reaction product (in this case $Na_2Fe_2(SO_4)_3$) exhibit lower decomposition temperature comparing with the substrates. From the above studies, it can be concluded that the 300 °C–400 °C temperature range is optimal in order to obtain $Na_{2+2y}Fe_{2-y}(SO_4)_3$ using Na_2SO_4 and $FeSO_4$.

4. Structural properties of $Na_2Fe_2(SO_4)_3$ and $Na_{2.5}Fe_{1.75}(SO_4)_3$ synthesised in different conditions

In order to investigate the influence of the synthesis condition on the structural properties of $Na_2Fe_2(SO_4)_3$, the studies involving the preparation of the material at 350 °C under different gas flows were performed. An inert atmosphere was realised by Ar flow, weakly and strongly reducing conditions were obtained by using Ar + 1%H_2 and Ar + 5%H_2 gas mixtures respectively. XRD data of synthesised $Na_2Fe_2(SO_4)_3$ are depicted in Fig. 2a. A collected patterns diffraction peaks can be indexed based on monoclinic crystal system with C2/c space group, characteristic for alluaudite structure. In all cases, additional peaks were observed, typical for Fe_3O_4 and $Fe_2(SO_4)_3$ structures, indicating the existence of these secondary phases in the final product (the phase compositions of the obtained powders are gathered in Table 1). As may be noted the amount of the impurities varies from 25 to 14 wt% with the smallest value for $Na_2Fe_2(SO_4)_3$ synthesised at strongly reducing atmosphere (Ar + 5%H_2). The existence of secondary phases is in a good agreement with literature data [10] and is believed to be due to the instability of stoichiometric $Na_2Fe_2(SO_4)_3$. As was recently reported the amount of the impurities can be reduced by simply changing the stoichiometry in $Na_{2+2y}Fe_{2-y}(SO_4)_3$ and producing the Na-rich material. This non-stoichiometry compound is assumed to be a one-to-one substitution of Fe by Na and excess Na in Na2 (Wyckoff position 4b) and Na3 (Wyckoff position 4e) sites for charge neutrality. Thus we synthesised $Na_{2.5}Fe_{1.75}(SO_4)_3$ compound which formula can written as $[Na1]_{1.0}[Na2]_{0.71}[Na3]_{0.54}[Fe_{0.875}Na_{0.125}]_2(SO_4)_3$ [18]. The Na-rich phase was produced at 350 °C using the strongly reducing gas mixture (Ar-5% H_2) since for this conditions the stoichiometric alluaudite compound exhibited the least amount of the impurities. As a result, we obtained the alluaudite phase with C2/c space group with additional peaks from the $Fe_2(SO_4)_3$ (Fig. 2b). The amount of impurities was reduced to 4 wt% in comparison to $Na_2Fe_2(SO_4)_3$ (Table 1). Taking into account the significant contribution of the synthesis conditions on the purity of obtained materials, fabrication of $Na_2Fe_2(SO_4)_3$ samples in a more reductive environment was undertaken. The synthesis with longer annealing time (30 h) and under the reductive atmosphere (Ar + 5% H_2) was performed. It was found that in the obtained samples after longer annealing time only reflection coming from Na_2SO_4 and FeS are present while no signature of the $Na_2Fe_2(SO_4)_3$ phase was detected. The XRD pattern with Rietveld refinement has been included in the supporting information (Fig. 1).

Additionally, the inductively coupled plasma atomic emission spectroscopy ICP was used in order to fully describe the composition of

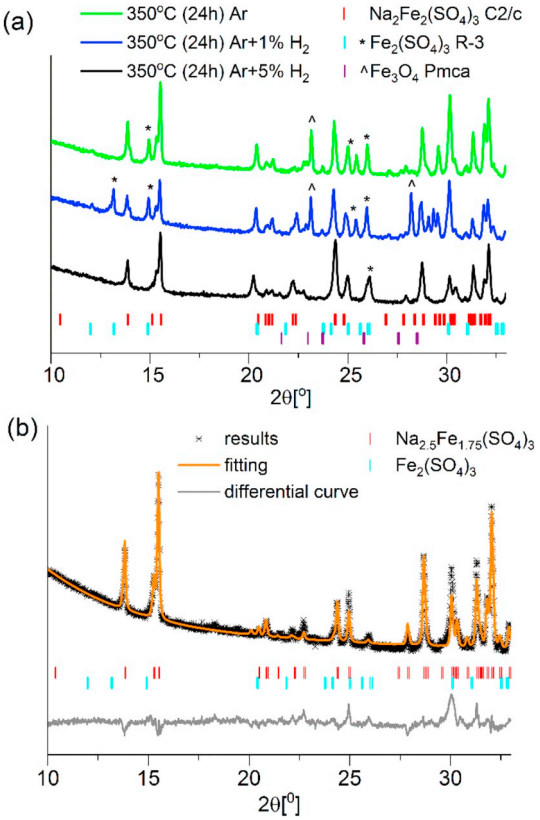

Fig. 2. The X-Ray diffraction patterns of (a) $Na_2Fe_2(SO_4)_3$ for different synthesis conditions and (b) $Na_{2.5}Fe_{1.75}(SO_4)_3$.

Table 1
The amount of impurities in synthesised $Na_{2+2y}Fe_{2-y}(SO_4)_3$ (NFS) (y = 0; 0.25) materials and Rp, Rwp, $\chi 2$ factors.

Compounds	Amount of NFS phase [%]	Amount of Fe_3O_4 phase [%]	Amount of $Fe_2(SO_4)_3$ phase [%]	Rp [%]	Rwp [%]	χ^2
$Na_2Fe_2(SO_4)_3$ synthesis in Ar flow	75	16	9	0.024	0.040	13.800
$Na_2Fe_2(SO_4)_3$ synthesis in Ar + 1%H_2 flow	81	6	13	0.018	0.0314	8.278
$Na_2Fe_2(SO_4)_3$ synthesis in Ar + 5%H_2 flow	86	2	12	0.021	0.033	9.612
$Na_{2.5}Fe_{1.75}(SO_4)_3$ synthesis in Ar + 5%H_2 flow	96	0	4	0.015	0.024	5.383

the $Na_2Fe_2(SO_4)_3$ sample synthesised in Ar + 5%H_2 atmosphere. The results indicate that obtained material has stoichiometry $Na_{1.97}Fe_{2.01}(SO_4)_3$. Taking into account measurement errors and fact that the determined stoichiometry is almost 2: 2 (Na: Fe) for the further discussion we name this compound $Na_2Fe_2(SO_4)_3$.

5. Microstructural analysis and grain size distribution of $Na_{2.5}Fe_{1.75}(SO_4)_3$

Scanning electron microscopy measurements (SEM) were performed in order to study the morphology of $Na_{2.5}Fe_{1.75}(SO_4)_3$. Fig. 3a presents SEM micrograph with the morphology of the examined sample. The investigated powder was found to possess spherical-shaped aggregates composed of heterogeneous particles which size varies in the 20 nm to 15 μm range. In the case of $Na_2Fe_2(SO_4)_3$ similar grain size and morphology of the powders were observed [7,19].

Energy dispersive spectroscopy analysis (EDS) of alluaudite Na-rich sample showed element compositions equal 2.5: 1.56 (Na: Fe) which is similar with theoretical ratio 2.5: 1.75 for $Na_{2.5}Fe_{1.75}(SO_4)_3$ and

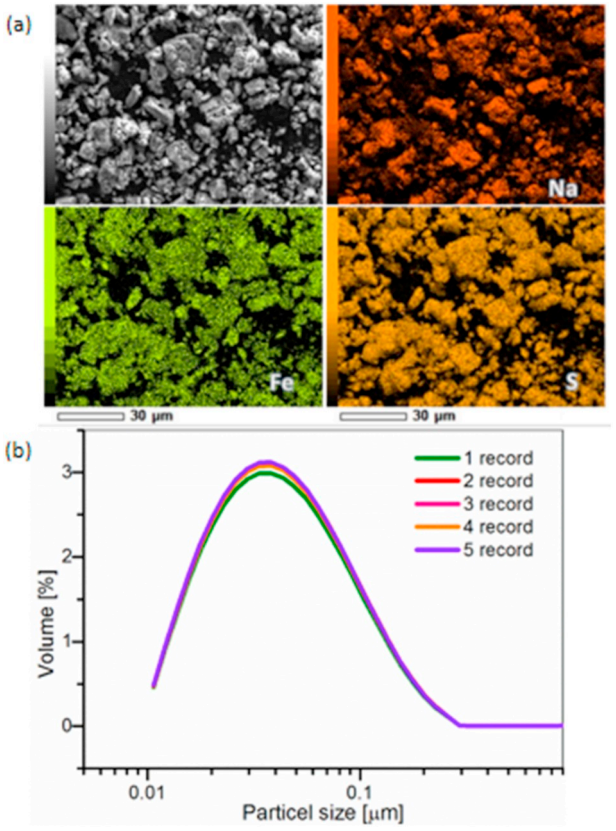

Fig. 3. (a) SEM/EDS images of $Na_{2.5}Fe_{1.75}(SO_4)_3$ with element mapping for Na, Fe, S atoms. (b) Grain size distribution of $Na_{2.5}Fe_{1.75}(SO_4)_3$ during five measurements.

therefore confirm the existence of the Na-rich and Fe-deficient composition in the final product. Furthermore, EDS analysis with element mapping for Na, Fe, S atoms led to the verification of uniform distribution of all constituent elements.

In addition, particle size distribution was measured. The observed distribution is shown in Fig. 3b. In the obtained $Na_{2.5}Fe_{1.75}(SO_4)_3$ sample most of the grains were smaller than 100 nm. This nanoscale morphology and nanometric grains can be rooted in the low temperature annealing (350 °C) involving less aggressive grain-growth, developing smaller particles.

6. Transport properties of $Na_{2.5}Fe_{1.75}(SO_4)_3$

Electrical conductivity (σ) of $Na_{2.5}Fe_{1.75}(SO_4)_3$ as a function of temperature (Fig. 4a) exhibits the thermally activated character with its value at room temperature around $2.4{\cdot}10^{-8}$ S cm^{-1}. One can observe a different type of σ character in 25 °C–300 °C and 300 °C–400 °C regimes. At lower temperatures, the electrical conductivity has activation energy (E_a) equals 0.44 eV whereas above 300 °C the slope of the σ becomes steeper and calculated E_a increases to 0.78 eV.

The recent DFT calculations [20] showed that the energy gap value for the fully sodiated $Na_2Fe_2(SO_4)_3$ has been determined as 3.58 eV defining its insulator behaviour. The density of state function revealed completely filled valence band with Fermi level just above the apex of this band and the empty conduction band. Furthermore, recent research [21] proves that electrical conductivity in $Na_{2.56}Fe_{1.72}(SO_4)_3$ sample is mainly governed by the ionic transport properties (98.8% ionic transference number). In the alluaudite structure the Na ions occupy three different crystallographic positions (Na1, Na2, Na3 as shown in Fig. 4b) and according to DFT calculation [9] the Na^+ migration will be essentially one-dimensional along the 001 direction and follows the Na3–Na3 pathway channel, due to a low activation energy of ca. 0.3 eV. The Na-ions may also migrate from the nominally fully occupied Na1 sites to the Na3 channels with activation energy estimated to 0.8 eV. For the Na2 positions, DFT model predicts separate strictly one-dimensional diffusion paths along the 001 direction with an activation energy of 0.6 eV.

Though it can be speculated that at low temperature regime 25 °C–300 °C (observed activation energy = 0.44 eV) sodium diffusion is dominated by the conduction mechanism with the lowest migration barrier 0.3 eV, i.e. migration of Na ions within Na3–Na3 channels. When the temperature exceeds the 300 °C energy of thermal oscillation is big enough to enable sodium ions to move from Na1 position to the Na3 chains and also permit sodium ions to become mobile within the separate Na2–Na2 channels. Since the observed activation energies of electrical conductivity (0.44 and 0.78 eV) are increased by relatively constant value comparing with calculated migration barriers of Na ions (0.3 and 0.6 eV) it may suggest the existence of some additional interaction between Na ions and electrons similar to those observed in iron phosphates [22,23].

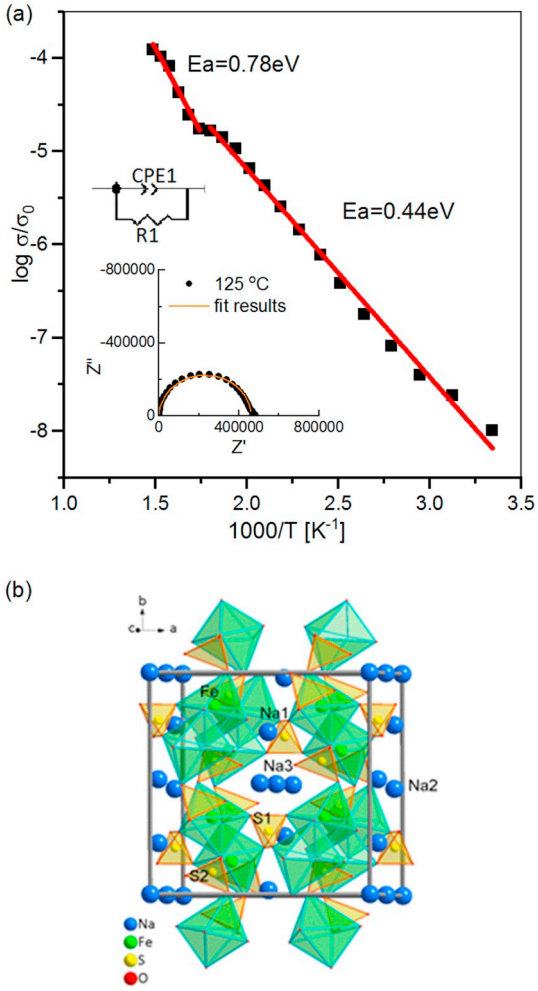

Fig. 4. (a) Electrical conductivity of $Na_{2.5}Fe_{1.75}(SO_4)_3$ measured with an Au/$Na_{2.5}Fe_{1.75}(SO_4)_3$/Au cell and (b) schematic crystal structure of $Na_2Fe_2(SO_4)_3$.

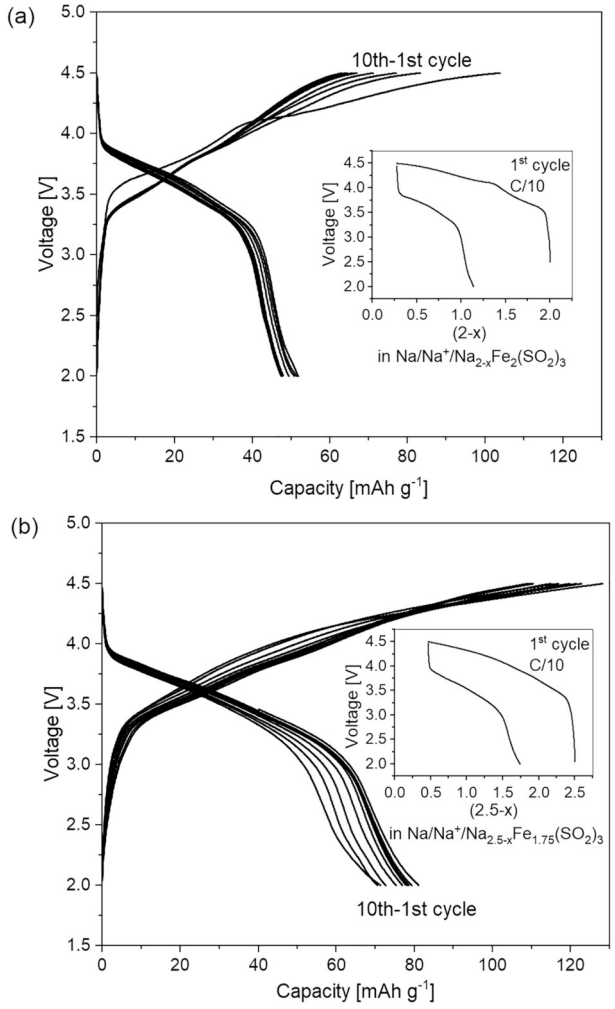

Fig. 5. Charge/discharge profiles for (a) Na/Na^+/$Na_{2-x}Fe_2(SO_4)_3$ and (b) Na/Na^+/$Na_{2.5-x}Fe_{1.75}(SO_4)_3$ at the rate of C/10.

7. Electrochemical properties of the $Na_{2+2y}Fe_{2-y}(SO_4)_3$ (y = 0; 0.25) cathode materials

The voltage profiles for the cells with $Na_2Fe_2(SO_4)_3$ and $Na_{2.5}Fe_{1.75}(SO_4)_3$ electrodes (with 1 M $NaPF_6$ in EC/DEC (1:1 vol. ratio) electrolyte) for first ten galvanostatic cycles in 2.0–4.5 V potential range (C/10 rate) are shown in Fig. 5.

Both cells exhibit an average voltage of 3.7 V (versus Na/Na^+) connected with the potential of the Fe^{3+}/Fe^{2+} redox couple. In case of Na/Na^+/$Na_{2-x}Fe_2(SO_4)_3$ the shape of the voltage profile for first charge process is significantly different compared with subsequent cycles, which may indicate some irreversible structural reorganization as found in case of $Li_2FeP_2O_7$ and Li_2FeSiO_4 [24,25]. Interestingly, for Na/Na^+/$Na_{2.5-x}Fe_{1.75}(SO_4)_3$ voltage characteristic of the first charge process is similar to the following ones which may point out that, contrary to the $Na_{2-x}Fe_2(SO_4)_3$, the crystal structure of the cathode material remains unchanged. Such behaviour may evidence that Na-rich phase of this alluaudite structure is more stable in battery working conditions. It corresponds well with the crystal structure results of the synthesised materials, revealing that $Na_{2.5}Fe_{1.75}(SO_4)_3$ can be obtained with much less amount of the impurities and as such may evidence higher thermodynamic stability of Na-rich phase. Both electrodes after first charge process show monotonous discharge curve in the 3.9 to 3.3 V voltage range which may suggest a single phase Na-ion intercalation reaction mechanism. The Na/Na^+/$Na_{2-x}Fe_2(SO_4)_3$ cell exhibits charge and discharge capacities equal to 70 and 50 mAh g^{-1} respectively, which corresponds to about 42% of its theoretical value (ca. 120 mAh g^{-1}) based on Fe^{3+}/Fe^{2+} redox couple. For Na-rich composition, the discharge capacity was found to be over 50% higher than for $Na_2Fe_2(SO_4)_3$ and reached 80 mAh g^{-1}. Non-Faradic reactions are observed during initial charging but after first cycle charge capacity reduces to lower values. Although non-negligible Faradaic loss upon charging is observed (higher charge capacity then discharge one) the observed values remain stable during performed cycles as can be seen in Fig. 6. Although stoichiometric material $Na_2Fe_2(SO_4)_3$ shows a higher theoretical capacity in comparison with $Na_{2.5}Fe_{1.75}(SO_4)_3$ (due to higher iron content), recorded values of these two systems are much better for Na-rich phase. It may be linked with the lower impurity concentration in $Na_{2.5}Fe_{1.75}(SO_4)_3$ as well as its higher structural stability.

With the intention to investigate the influence of the electrolyte on the reversibility of the electrode processes as well as discharge capacities of the investigated materials, we perform various charge/discharge tests of the Na/Na^+/$Na_{2.5-x}Fe_{1.75}(SO_4)_3$ cells. Firstly, we check the influence of the three types of electrolytes: 1 M $NaPF_6$ in EC:DEC (1:1 vol. ratio), 1 M $NaPF_6$ in PC and 1 M $NaClO_4$ in PC, on electrochemical activity of examined systems. Electrode discharge capacities as a function of cycle number for cells with various electrolytes are shown in Fig. 7a. Interestingly, the highest value – 80 mAh g^{-1} is observed for 1 M $NaPF_6$ in EC:DEC electrolyte, whereas in two other cases considerably lower capacities are a recorder, that is 50 and 35 mAh g^{-1} for 1 M $NaPF_6$ in PC and 1 M $NaClO_4$ in PC respectively. Nevertheless,

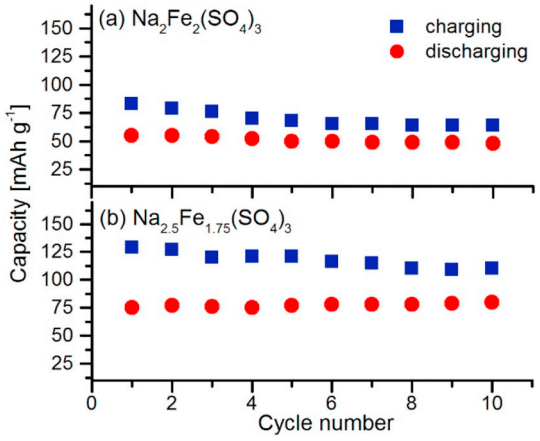

Fig. 6. Evolution of capacity as a function of cycle number for (a) $Na_2Fe_2(SO_4)_3$ and (b) $Na_{2.5}Fe_{1.75}(SO_4)_3$ cathodes.

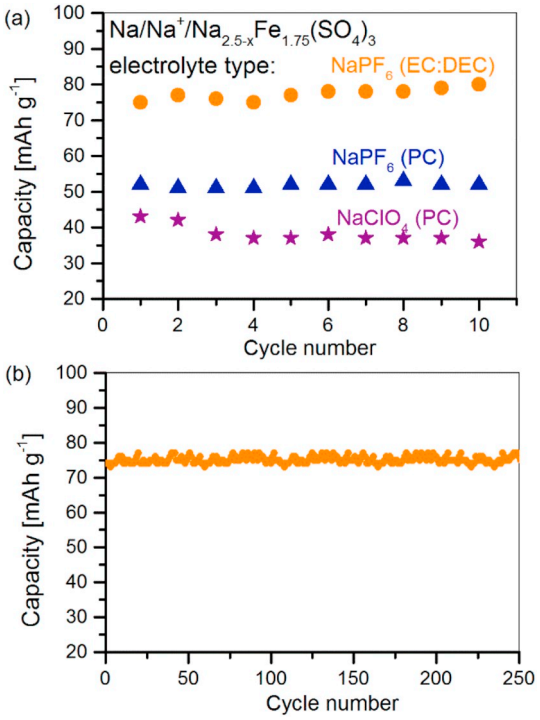

Fig. 7. (a) Evolution of capacity of $Na/Na^+/Na_{2.5-x}Fe_{1.75}(SO_4)_3$ cells with various electrolytes (discharge at the rate of C/10). (b) Discharge capacity of the $Na/Na^+/Na_{2.5-x}Fe_{1.75}(SO_4)_3$ cell during long term charge/discharge tests (charge/discharge rates C/10).

for all systems stable values of the discharge capacities are obtained throughout all the charge/discharge tests, indicating good stability of the investigated $Na_{2.5}Fe_{1.75}(SO_4)_3$ material in contact with examined electrolytes. In order to investigate the long-term performance of the alluaudite cathode, the extended charge/discharge tests were performed. Fig. 7b presents the recorded discharge capacity of the $Na/Na^+/Na_{2.5-x}Fe_{1.75}(SO_4)_3$ cell with C/10 discharge rate. As can be seen, the obtained values remain stable and are close to 75 mAh g^{-1} throughout the all types of test, the relative decrease of the discharge capacity was estimated to be 2% after 250 cycles, which can be associated with the facile Na transport within the sodium diffusion channels and robust 3D structure formed by the SO_4^{2-}. This very small capacity fade indicates good cycling stability of the material despite the high operating voltage and non-negligible Faradaic loss upon charging.

In Fig. 8 cyclic voltammograms for Na-ion type cells with

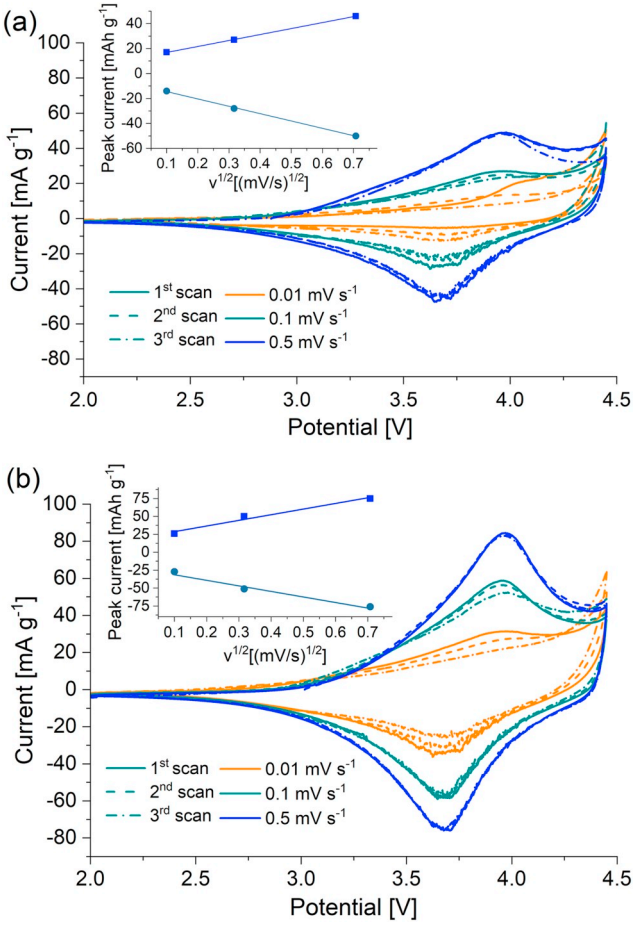

Fig. 8. Cyclic voltammetry plots for (a) $Na/Na^+/Na_{2-x}Fe_2(SO_4)_3$ (b) $Na/Na^+/Na_{2.5-x}Fe_{1.75}(SO_4)_3$ cell for different scanning rates 0.02 mV s^{-1}, 0.05 mV s^{-1} and 0.1 mV s^{-1}.

$Na_{2+2y}Fe_{2-y}(SO_4)_3$ electrodes (with 1 M $NaPF_6$ in EC/DEC electrolyte) with 0.01, 0.1, 0.5 mV s^{-1} scanning rates (υ) are depicted. In case of as assembled $Na/Na^+/Na_{2-x}Fe_2(SO_4)_3$ cell (Fig. 8a), cathode peak around 4.1 V observed during the first run (0.01 mV s^{-1} rate) disappears in subsequent cycles along with the appearance of another cathode peak at 3.9 V. For $Na/Na^+/Na_{2.5-x}Fe_{1.75}(SO_4)_3$ cell (Fig. 8b) one cathode (3.9 V) and one anode peak (3.6 V) are clearly visible in all tests with three scanning rates. It may be speculated that the observed cathode and anode peaks present at 3.9 and 3.6 V corresponds to the sodium intercalation and deintercalation processes involving Fe^{3+}/Fe^{2+} redox couple. For both cells for higher scanning rates: 0.1 and 0.5 mV s^{-1} the increase of the peak currents and a slight shift of its positions on the voltage scale are observed. Similarly, to the charge/discharge tests in case of the $Na_2Fe_2(SO_4)_3$ the current-voltage characteristics during first CV cycle are slightly different from those in the subsequent cycles, while $Na_{2.5}Fe_{1.75}(SO_4)_3$ electrode exhibits the same current-voltage characteristics during all CV measurements.

In order to further investigate the kinetics behaviour of both materials the current values for anode and cathode peaks were plotted vs. root square of the scanning rate ($\upsilon^{1/2}$). As can be seen, the obtained values (insets in Fig. 8a and b) shows linear dependence as a function of $\upsilon^{1/2}$ which suggests that within the operating conditions the electrode reactions are diffusion-limited. The symmetrical characteristics of anode and cathode peaks currents indicate good reversibility of the sodium insertion/deinsertion reactions, which may be understood taking into consideration the existence of the fast-diffusion path formed by the open crystallographic channels along the *c* direction. Since the electrode reaction is diffusion-limited, obtained data were used to

Table 2
The value of sodium chemical diffusion coefficients for $Na_2Fe_2(SO_4)_3$ and $Na_{2.5}Fe_{1.75}(SO_4)_3$.

	$Na_2Fe_2(SO_4)_3$	$Na_{2.5}Fe_{1.75}(SO_4)_3$
Diffusion coefficients (10^{-9} cm^2 s^{-1})	1.49	2.31

calculate the sodium chemical diffusion coefficients ($\widetilde{D_{Na}}$) according to the expression of the peak current i_P (A) for the forward sweep in a reversible system given by the Randles–Sevcik equation [26,27]:

$$i_P = 0.4463 \bullet n \bullet F \bullet A \bullet C \bullet \left(\frac{n \bullet F \bullet \upsilon \bullet \widetilde{D_{Na}}}{R \bullet T} \right)^{1/2}$$

where n is the number of electron equivalent exchanged during the redox process (n = 1), A (cm^2) the active area of the working electrode, C (mol cm^{-3}) concentration of the ions within the bulk, F (96 485 C mol^{-1}) Faraday constant, υ (V s^{-1}) voltage scanning rate, R (8.314 J mol^{-1} K^{-1}) gas constant, T (295 K) temperature and $\widetilde{D_{Na}}$ (cm^2 s^{-1}) sodium chemical diffusion coefficient.

The C - concentration of the sodium ions for $Na_{2+2y}Fe_{2-y}(SO_4)_3$ electrodes were calculated taking into consideration occupancy of the Na ions in the 4b and 4e Wyckoff positions within C2/c alluaudite structure. For $Na_2Fe_2(SO_4)_3$ and $Na_{2.5}Fe_{1.75}(SO_4)_3$ concentrations were estimated to be equal 0.015 and 0.018 mol cm^{-3} (firstly the precise number of the Na – ions within the single unit cells in $Na_{2+2y}Fe_{2-y}(SO_4)_3$ were estimated and then obtained quantities were divided by the unit cell volume (in cm^3) and Avogadro number) respectively. The active area A (cm^2) of the working electrode was valued 40 cm^2 basing on the BET measurements (about 20 m^2 g^{-1}) and the mass of the active material in the investigated cells. Calculated values of the sodium chemical diffusion coefficients ($\widetilde{D_{Na}}$) (cm^2 s^{-1}) at room temperature based on the linear fitting of the obtained data for investigated electrodes are gathered in Table 2.

The calculated $\widetilde{D_{Na}}$ are on the order of 10^{-9} cm^2 s^{-1}, with the about two times bigger values for $Na_{2.5}Fe_{1.75}(SO_4)_3$ than $Na_2Fe_2(SO_4)_3$. These numbers of the Na ion diffusion coefficients are relatively high which may be once again subscribed to the existence of the fast-diffusion path formed by the open crystallographic channels along the *c* direction of the alluaudite structures.

8. Conclusion

This study presents an evaluation of the optimal synthesis conditions for $Na_{2+2y}Fe_{2-y}(SO_4)_3$ cathode material. For the first time using thermogravimetric measurement with mass spectrometry, we determined the temperature range (300 °C–400 °C) at which $Na_{2+2y}Fe_{2-y}(SO_4)_3$ can be synthesised. Our research also proved that it is beneficial to synthesise $Na_{2+2y}Fe_{2-y}(SO_4)_3$ under highly reducing conditions. In previous works, alluaudite materials were obtained in argon atmosphere while we point out that the scenario leading to the least amount of the impurities is annealing under the Ar + 5%H_2 flow. We fabricated the non-stoichiometric material $Na_{2.5}Fe_{1.75}(SO_4)_3$ with 4 wt% of impurities, which is similar to literature data, but comparing with synthesis procedures provided till now, annealing of the alluaudite materials in a highly reducing atmosphere significantly shortens the grinding time and allows grinding in the air instead of argon. The obtained capacity for $Na/Na^+/Na_{2.5-x}Fe_{1.75}(SO_4)_3$ cell (80 mAh g^{-1}) agrees with the assumed theoretical capacity for non-stoichiometric material [28]. Electrical conductivity results for $Na_{2.5}Fe_{1.75}(SO_4)_3$ material in its thermal stability range (25 °C–400 °C) was reported. The change in the nature of the electrical conductivity with an increase of the temperature was observed. It was proposed that modification of the conduction mechanism can be connected with the different sodium diffusions path (within Na3–Na3 and Na2–Na2 channels) which was in good agreement with Na-ion diffusion modeling [9]. Additionally, the electrode reaction kinetics of the $Na_{2+2y}Fe_{2-y}(SO_4)_3$ electrodes were evaluated by means of the CV studies accomplished with the sodium chemical diffusion coefficients ($\widetilde{D_{Na}}$) calculation basing on the Randles–Sevcik approach. The comprehensive investigation of the transport properties of $Na_{2.5}Fe_{1.75}(SO_4)_3$ material enables to put forward the hypothesis that electronic part of the mixed ionic-electronic conductivity is the factor limiting the performance of the electrode.

Supplementary data to this article can be found online at https://doi.org/10.1016/j.ssi.2019.02.007.

Acknowledgments

Work was supported by the National Science Centre Poland (NCN) of the basis of the decisions number 2016/21/D/ST5/01658 and Polish Ministry of Science and Higher Education, under project AGH No. 15.11.210.398.

References

[1] B.L. Ellis, L.F. Nazar, Sodium and sodium-ion energy storage batteries, Curr. Opin. Solid State Mater. Sci. 16 (2012) 168–177, https://doi.org/10.1016/j.cossms.2012.04.002.
[2] M.D. Slater, D. Kim, E. Lee, C.S. Johnson, Sodium-ion batteries, Adv. Funct. Mater. 23 (2013) 947–958, https://doi.org/10.1002/adfm.201200691.
[3] D. Baster, K. Dybko, M. Szot, K. Świerczek, J. Molenda, Sodium intercalation in NaxCoO2−y — correlation between crystal structure, oxygen nonstoichiometry and electrochemical properties, Solid State Ionics 262 (2014) 206–210, https://doi.org/10.1016/j.ssi.2013.11.040.
[4] Y. Li, Y. Lu, C. Zhao, Y.S. Hu, M.M. Titrici, H. Li, X. Huang, L. Chen, Recent advances of electrode materials for low-cost sodium-ion batteries towards practical application for grid energy storage, Energy Storage Mater. 7 (2017) 130–151, https://doi.org/10.1016/j.ensm.2017.01.002.
[5] G. Sheng-Ping, L. Jia-Chuang, X. Qian-Ting, M. Ze, X. Huai-Guo, Recent achievements on polyanion-type compounds for sodium-ion batteries: syntheses, crystal chemistry and electrochemical performance, J. Power Sources 361 (2017) 285–299, https://doi.org/10.1016/J.JPOWSOUR.2017.07.002.
[6] S.W. Kim, D.H. Seo, X. Ma, G. Ceder, K. Kang, Electrode materials for rechargeable sodium-ion batteries: potential alternatives to current lithium-ion batteries, Adv. Energy Mater. 2 (2012) 710–721, https://doi.org/10.1002/aenm.201200026.
[7] P. Barpanda, G. Oyama, S. Nishimura, S.-C. Chung, A. Yamada, A 3.8-V earth-abundant sodium battery electrode, Nat. Commun. 5 (2014) 1–8, https://doi.org/10.1038/ncomms5358.
[8] J. Ming, P. Barpanda, S.I. Nishimura, M. Okubo, A. Yamada, An alluaudite Na2 + 2xFe2-x(SO4)3(x = 0.2) derivative phase as insertion host for lithium battery, Electrochem. Commun. 51 (2015) 19–22, https://doi.org/10.1016/j.elecom.2014.11.009.
[9] L.L. Wong, H.M. Chen, S. Adams, Sodium-ion diffusion mechanisms in the low cost high voltage cathode material $Na_{2+\delta}Fe_{2-\delta/2}(SO_4)_3$, Phys. Chem. Chem. Phys. 17 (2015) 9186–9193, https://doi.org/10.1039/C5CP00380F.
[10] G. Oyama, S. Nishimura, Y. Suzuki, M. Okubo, A. Yamada, Off-stoichiometry in alluaudite-type sodium iron sulfate Na2 + 2xFe2 − x(SO4)3 as an advanced sodium battery cathode material, ChemElectroChem 2 (2015) 1019–1023, https://doi.org/10.1002/celc.201500036.
[11] GSAS xrd software, https://Subversion.Xray.Aps.Anl.Gov/Trac/PyGSAS (n.d.).
[12] A.C. Larson, General structure analysis system (GSAS), Los Alamos Lab. Rep. 748 (1994) 86–748, https://doi.org/10.1103/PhysRevLett.101.107006.
[13] B.H. Toby, EXPGUI, a graphical user interface for GSAS, J. Appl. Crystallogr. 34 (2001) 210–213, https://doi.org/10.1107/S0021889801002242.
[14] T.P. Prasad, Kinetics of thermal decomposition of intermediate hydrates and basic salts of iron(II) sulphate heptahydrate, J. Therm. Anal. 31 (1986) 553–557, https://doi.org/10.1007/BF01914231.
[15] T. Wang, K.A. Debelak, J.A. Roth, Dehydration of iron(II) sulfate heptahydrate, Thermochim. Acta 462 (2007) 89–93, https://doi.org/10.1016/j.tca.2007.07.001.
[16] S. Yang, W. Du, P. Shi, J. Shangguan, S. Liu, C. Zhou, P. Chen, Q. Zhang, H. Fan, Mechanistic and kinetic analysis of Na2SO4 -modified laterite decomposition by thermogravimetry coupled with mass spectrometry, PLoS One 11 (2016) 1–21, https://doi.org/10.1371/journal.pone.0157369.
[17] J.C. Halle, K.H. Stern, Vaporization and decomposition of Na2SO4. Thermodynamics and kinetics, J. Phys. Chem. 84 (1980) 1699–1704, https://doi.org/10.1021/j100450a007.
[18] S. Nishimura, Y. Suzuki, J. Lu, S. Torii, T. Kamiyama, A. Yamada, High-temperature neutron and X-ray diffraction study of fast sodium transport in alluaudite-type sodium iron sulfate, Chem. Mater. 28 (2016) 2393–2399, https://doi.org/10.1021/acs.chemmater.6b00604.
[19] D. Dwibedi, R.B. Araujo, S. Chakraborty, P.P. Shanbogh, N.G. Sundaram, R. Ahuja, P. Barpanda, Na2.44Mn1.79(SO4)3: a new member of the alluaudite family of insertion compounds for sodium ion batteries, J. Mater. Chem. A 3 (2015) 18564–18571, https://doi.org/10.1039/C5TA04527D.
[20] R.B. Araujo, S. Chakraborty, P. Barpanda, R. Ahuja, Na2M2(SO2)3 (M = Fe, Mn, Co

and Ni): towards high-voltage sodium battery applications, Phys. Chem. Chem. Phys. 18 (2016) 9658–9665, https://doi.org/10.1039/C6CP00070C.
[21] J. Lu, A. Yamada, Ionic and electronic transport in alluaudite Na2 + 2x Fe2-x(SO4)3, ChemElectroChem 3 (2016) 902–905, https://doi.org/10.1002/celc.201500535.
[22] B. Ellis, L.K. Perry, D.H. Ryan, L.F. Nazar, Small polaron hopping in LixFePO4 solid solutions: coupled lithium-ion and electron mobility, J. Am. Chem. Soc. 128 (2006) 11416–11422, https://doi.org/10.1021/ja0614114.
[23] H.J. Tan, J.L. Dodd, B. Fultz, Mössbauer spectrometry study of thermally-activated electronic processes in Li x FePO 4, J. Phys. Chem. C 113 (2009) 2526–2531, https://doi.org/10.1021/jp808537z.
[24] B. Zhang, X. Ou, J.C. Zheng, C. Shen, L. Ming, Y.D. Han, J.L. Wang, S.E. Qin, Electrochemical properties of Li2FeP2O7 cathode material synthesized by using different lithium sources, Electrochim. Acta 133 (2014) 1–7, https://doi.org/10.1016/j.electacta.2014.03.188.
[25] A. Nytén, A. Abouimrane, M. Armand, T. Gustafsson, J.O. Thomas, Electrochemical performance of Li2FeSiO4 as a new Li-battery cathode material, Electrochem. Commun. 7 (2005) 156–160, https://doi.org/10.1016/j.elecom.2004.11.008.
[26] A.J. Bard, L.R. Faulkner, Electrochemical Methods Fundamentals and Applications, (1944), https://doi.org/10.1016/B978-0-12-381373-2.00056-9.
[27] Y.-S. Lee, K.-S. Ryu, Study of the lithium diffusion properties and high rate performance of TiNb6O17 as an anode in lithium secondary battery, Sci. Rep. 7 (2017) 1–13, https://doi.org/10.1038/s41598-017-16711-9.
[28] P. Barpanda, Pursuit of sustainable iron-based sodium battery cathodes: two case studies, Chem. Mater. 28 (2016) 1006–1011, https://doi.org/10.1021/acs.chemmater.5b03926.